Kerr-Like Nonlinearity Induced via Terahertz Generation and the Electro-Optical Effect in Zinc Blende Crystals

J-P. Caumes,[1,2] L. Videau,[2] C. Rouyer,[2] and E. Freysz[1,*]

[1]Centre de Physique Moléculaire Optique et Hertzienne, Université Bordeaux I, 351, cours de la libération,
33405 Talence cedex, France

[2]Commissariat à l'Energie Atomique, Centre d'Etudes Scientifiques et Techniques d'Aquitaine, B.P. 2,
33114 Le Barp, France

A model is proposed to account for Kerr-like nonlinearity induced by femtosecond pulses via terahertz generation and electro-optical effect. This phenomenon, so far overlooked, is evidenced in a zinc blende single crystal with a heterodyne optical Kerr effect setup. The spectral evolution of this phenomenon as well as its noninstantaneous response character are reported. Its competition with a third-order optical Kerr effect is demonstrated.

The past ten years proposed different optoelectronic solutions based on Kerr-like nonlinearities. Besides the third-order nonlinear (TON) susceptibility, symmetrically allowed in all materials, cascaded second-order nonlinear (SON) effects occurring in noncentrosymmetric medium provide an efficient alternative for creating equivalent Kerr-like nonlinearities. For instance, in nearly phase-matched second harmonic generation (SHG), a large induced phase shift has been observed [1,2]. This phase shift results from a change of the index of refraction of a medium n which is defined as $n = n_0 + n_2 I$, where n_0 is the linear refractive index, n_2 is the nonlinear index of refraction, and I is the intensity of the incoming beam. Close to the phase-matching condition the nonlinear refractive index n_2 due to SHG, noted n_2^{SHG}, is adjustable in amplitude and sign. It can be made large compared to the one associated with the TON susceptibility $\chi^{(3)}$, noted n_2^{Kerr}.

Another equivalent way to induce a similar n_2 in a non-centrosymmetric medium, noted n_2^{OR}, is to consider the backaction of the optical rectified field upon the fundamental wave through the electro-optical effect [3]. Bosshard *et al.* [4] as well as Biaggio [5] recently revisited this phenomenon. To compute n_2^{OR} these authors took into account the static electric field due to the optical rectification of the laser pulse within an electro-optical crystal. While their analysis is valid for laser pulses of a few tens of a picosecond, it does not hold if subpicosecond laser pulses are used. Indeed, since the spectral width of a short laser pulse is large, the various spectral components of the pulse are mixed in the nonlinear crystal and can beat with each other (difference frequency mixing). This phenomenon generates terahertz (THz) radiations [6] which could also modify the index of refraction of the medium. For laser pulses below 100 fs, very broad THz radiations ($5 \ \mu m < \lambda^{THz} < 500 \ \mu m$) are propagated in the crystal. As in SHG, the coupling of this THz pulse with another SON coefficient (sum frequency mixing or electro-optical effect) gives rise to a novel nonlinear index of refraction noted n_2^{THz} which has so far been overlooked. It is important to note that, unlike the case discussed by [4,5] that is related to the static electric field induced in the medium, hereafter we are mainly interested in index change due to the propagation of THz radiation in the crystal. In this Letter, we will show that only the THz spectral components that almost fulfill the phase-matching condition contribute to n_2^{THz}. This is contrary to either the second harmonic where n_2^{SHG} is maximum when the phase-matching condition is not perfectly satisfied or static optical rectification where n_2^{OR} is always phase matched. Moreover, the large dispersion of the index of refraction in the THz spectral domain implies that n_2^{THz} is not instantaneous. Owing to the spectral dispersion of the THz components and depending on the sign of Δk^{THz} [7], THz spectral components can propagate with a phase velocity faster or slower than the group velocity $v_g(\omega)$ of the optical pulse. This implies that another weak femtosecond laser pulse can sense the index modulation after or even before the pump pulse leaves the crystal.

To evidence this phenomenon, we used a heterodyne optical Kerr experimental setup [8]. This time-resolved noncollinear ($\theta \sim 5°$) pump-probe experiment uses a continuously mode locked femtosecond Ti:sapphire oscillator (790 nm $< \lambda <$ 890 nm, $\tau_p = 100$ fs, 76 MHz). The index change induced by a linearly polarized pump beam is sensed by a probe pulse linearly polarized at 45° with respect to the pump beam. The temporal evolution of the small birefringence $\Delta\Phi(t) \sim n_2 I^{pu}(t)$ induced by the pump intensity I^{pu} and sensed by the time delayed probe beam is measured by a photodiode connected to a lock-in amplifier and placed along the probe beam propagation direction after the sample. The sample is inserted between two crossed polarizers. In front of the sample, tuning off the main axis of the $\lambda/4$ wave plate by a small angle α, called hereafter the heterodyne coefficient, introduces a weak ellipticity on the probe polarization: hence, a small part of the probe beam intensity I^{pr} leaks out

through the polarizer in front of the photodiode and allows a linear detection of the induced birefringence. For each time delay τ between the pump and probe pulses, the lock-in amplifier provides a temporally averaged signal $S(\tau) = \alpha \eta \langle \Delta\Phi(t)I^{\text{pr}}(t + \tau)\rangle$, where η is the light to the current conversion efficiency of the photodiode. We adjust the pump polarization using a $\lambda/2$ wave plate placed along the pump beam direction in front of the sample.

The heterodyne optical Kerr experiments were performed in ZnSe and ZnTe cubic single crystals cut along the $\langle 110 \rangle$ plane. They are optically isotropic and have large and well-known linear and nonlinear optical coefficients in the far infrared and in the visible region. They have only one non null second-order tensor coefficient $\chi^{(2)}_{ijk}$, where $i \neq j \neq k$, and two independent TON tensor coefficients $a = \chi^{(3)}_{iiii}$ and $b = \chi^{(3)}_{ijji} = \chi^{(3)}_{iijj} = \chi^{(3)}_{ijij}$, where $i \neq j$. Hereafter, we will note $u = \frac{\chi^{(3)}_{iiii}}{\chi^{(3)}_{ijij}}$.

In a crystal, the birefringence $\Delta\Phi$ is due to n_2 which is in general given by $n_2 = n_2^{\text{Kerr}} + n_2^{\text{SHG}} + n_2^{\text{OR}} + n_2^{\text{THz}}$. In practice, one needs to find a way to evaluate the amplitude of each contribution. In Table I, the reported values of n_2^{Kerr}, n_2^{OR}, and n_2^{SHG}, in ZnSe and ZnTe crystals, clearly indicate that n_2^{Kerr} always overcomes the contribution of n_2^{OR} and n_2^{SHG}. We will show that, under given experimental conditions, n_2^{THz} cannot be neglected compared to n_2^{Kerr}. Finally, it is important to recall that, according to the crystal symmetry, if the polarization of the laser pulses is along one of the crystal axes, $\Delta\Phi$ is due to n_2^{Kerr} only. This allows us to evaluate independently n_2^{Kerr}. Moreover, rotating the laser polarization away from the crystallographic axis makes it possible to record the evolution of n_2 due to the competition between n_2^{Kerr} and n_2^{THz}.

According to the above presented experiments, a three-wave mixing equation (pump, probe, and THz field) must be solved to analytically describe the recorded signal.

TABLE I. Nonlinear optical coefficients of ZnTe and ZnSe (see [4]).

	$\chi^{(2)}$ (m/V)	$\chi^{(3)}$ (m^2/V^2)	n_2^{Kerr} (m^2/W)	n_2^{SHG} (m^2/W)	n_2^{OR} (m^2/W)
ZnTe	90.10^{-12}	3.10^{-19}	1.10^{-17}	-5.10^{-20}	4.10^{-20}
ZnSe	30.10^{-12}	1.10^{-19}	3.10^{-18}	-2.10^{-20}	5.10^{-21}

Here we suppose that the pump laser pulse E^{pu} is not modified during its propagation in the nonlinear crystal. We write $E^{\text{pu}}(\omega, t, x, y, z) = F(x, y)S(t)e^{i(\omega\tau - kz)}$, where $F(x, y)$ and $S(t)$ are, respectively, the spatial and temporal dependence of the pump beam and ω is the central frequency of the pump pulse. The $\langle 001 \rangle$ crystallographic axis is along the y axis of the (x, y, z) Cartesian coordinates. At each point z of the medium, the difference frequency mixing between the different spectral components of the pump wave $E^{\text{pu}}(\omega, t, x, y, z)$ induces a TON polarization $P_i^{(2)}(\Omega, x, y, z) = \frac{\epsilon_0}{2\pi}\int \chi^{(2)}_{ijk}(\Omega, \omega, \Omega - \omega)E_j^{\text{pu}}(\Omega - \omega, x, y, z)E_k^{\text{pu}}(\omega, x, y, z)\,d\omega$, where ω and Ω lie, respectively, in the optical and THz frequency ranges. It radiates different spectral components of THz waves at frequencies Ω. The amplitude of each spectral THz component $E^{\text{THz}}(\Omega, k_x, k_y, z)$ is computed by solving the nonlinear Maxwell equation [9] in the spatial and temporal Fourier domains:

$$\frac{\partial^2}{\partial z^2}E^{\text{THz}}(\Omega, k_x, k_y, z) + [k(\Omega)^2 - k_\perp^2] \times$$
$$E^{\text{THz}}(\Omega, k_x, k_y, z) = H(\Omega)G(k_x, k_y)e^{i\Omega(z/v_g)} \quad (1)$$

with $G(k_x, k_y) = \frac{1}{4\pi^2}\int |F(x, y)|^2 e^{-i(k_x x + k_y y)}\,dxdy$, $H(\Omega) = -\frac{\Omega^2}{c^2}\chi^{(2)}(\Omega)C(\Omega)$, where $C(\Omega)$ is the Fourier transform of $|S(t)|^2$, $\chi^{(2)}(\Omega) = 2d_{14}(\Omega)$, $k_\perp^2 = k_x^2 + k_y^2$, v_g is the group velocity of the laser pulse, and c is the velocity of light in vacuum. The resolution of (1) yields the THz field at each point in the crystal:

$$E^{\text{THz}}(\Omega, k_x, k_y, z) = iz\frac{G(k_x, k_y)}{\sqrt{k(\Omega)^2 - k_\perp^2} + \frac{\Omega}{v_g}}\frac{\Omega^2}{c^2}\chi^{(2)}(\Omega)C(\Omega)e^{i(\Omega/v_g + \sqrt{k(\Omega)^2 - k_\perp^2})z/2}$$
$$\times \text{sinc}\left[\left(\sqrt{k(\Omega)^2 - k_\perp^2} - \frac{\Omega}{v_g}\right)\frac{z}{2}\right]. \quad (2)$$

For $k_x = k_y = 0$, we present in Figs. 1a and 1c the evolution of the THz power spectrum at the entrance $[I_{\text{en}}(\Omega)]$ and exit $[I_{\text{ex}}(\Omega)]$ of 2 mm ZnTe and ZnSe crystals excited by a 100 fs pulse whose central wavelength equals 800 nm.

As previously shown [6], if one neglects the dispersion of $\chi^{(2)}(\Omega)$, the strong modification of the THz spectrum at the exit of the crystal is basically the product of three contributions, the Ω^2 dependence of the radiative efficiency, the initial power spectrum of the rectified input laser pulse $C(\Omega)$, and the phase-matching curve represented by the sinc function. The combination of these three functions explains the peaked structure of $I_{\text{ex}}(\Omega)$ at $\Omega = 2.3$ THz for the ZnTe crystal, where the phase-matching condition is satisfied at $\Omega = 2.3$ THz. On the contrary, the behavior is different for the ZnSe crystal, where no THz spectral components are phase matched. In Figs. 1b and 1d, the temporal THz waveform at the exit of the crystal $E_{\text{ex}}^{\text{THz}}(t)$ is presented as well. In Fig. 1b, one notes first, for the ZnTe crystal, that at the end of the crystal a part of the THz wave leaves the crystal before the pump beam and, second, that the THz maximum is delayed in time with respect to the laser pulse. This behavior is related to the fact that $v_{(\phi)}(\Omega > 2\text{ THz})$ and $v_{(\phi)}(\Omega < 2\text{ THz})$ of the THz component are respectively, higher and lower than $v_g(\omega)$. Such behavior cannot be recorded in the ZnSe crystal, where, whatever Ω, $v_{(\phi)}(\Omega) < v_g(\omega)$ (Fig. 1d). Knowing the temporal evolution of the THz field at each point of the medium, we computed the phase shift,
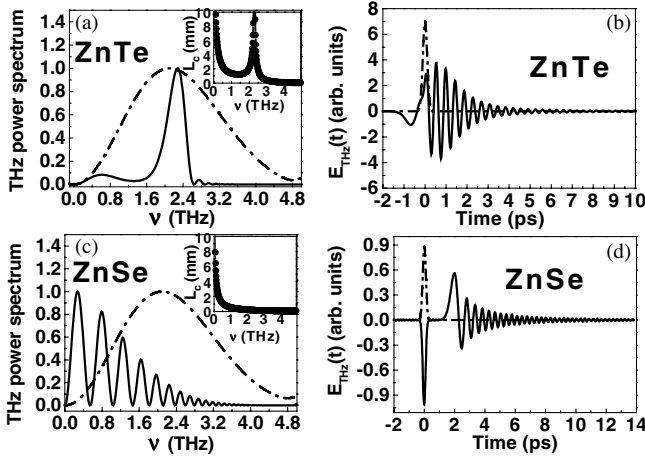
FIG. 1. (a,c): Calculated $I_{en}^{THz}(\Omega)$ (dash-dotted lines) and $I_{ex}^{THz}(\Omega)$ (solid lines) for ZnTe (a) and ZnSe (c). The insets represent the evolution of the coherence length $L_c(\nu) = \pi/\Delta k^{THz}(\nu)$. (b,d): Calculated $E_{ex}^{THz}(t)$ (solid lines). The dash-dotted lines represent the pump wave. All the figures have been calculated accounting for the dispersion of $\chi^{(2)}(\Omega)$.

sensed by the probe wave propagating along the z axis (i.e. $k_x = k_y = 0$) and induced by both the SON and TON polarizations $P_i^{(2)}(z,t) = \epsilon_0 c_{ijk}^{(2)} E_j^{THz}(z,t) E_k^{pr}(z,t)$

and $P_i^{(3)}(z,t) = \epsilon_0 c_{ijkl}^{(3)} E_j^{pu}(z,t) E_k^{pu}(z,t) E_l^{pr}(z,t)$, respectively. The slowly varying amplitude of the probe wave A_{pr} yields

$$\frac{\partial A_i^{pr}(T,z)}{\partial z} = i \frac{\omega^2}{2k\epsilon_0 c^2}[P_i^{(2)}(T,z) + P_i^{(3)}(T,z)], \quad (3)$$

where $T = t + \frac{z}{v_g}$ and $i = x$ or y. We recall that, in the slowly varying amplitude approximation, the second-order polarization writes $P_i^{(2)} = \epsilon_0 c_{ijk}^{(2)} E^{THz}(z,t) A^{pr}(z,t)$, where c_{ijk} and c_{ijkl} are the Fourier transform of χ_{ijk} and χ_{ijkl}. This polarization, which depends on both the phase and the amplitude of the THz wave, modifies the index of refraction seen by the probe beam. Since both the third- and second-order nonlinear polarizations modify differently the index seen by the x and y components of the probe wave, the initially linear polarization of the probe beam becomes slightly elliptical after its propagation in the crystal. This elliptic polarization is evidenced by the time-resolved optical Kerr effect experiment and gives rise to the signal $S(\tau)$. To compare our model with experimental data, we computed the signal recorded at the exit of the crystal by the lock-in amplifier. Considering that only either second- or third-order polarizations are responsible for the observed phenomena, we obtained

$$S^{(Kerr)}(\tau) = \frac{3bL\omega^2\alpha}{kc^2}[(u+1)\cos^2(\Psi) - 2(u-1)\sin^2(\Psi)] \int |I^{pu}(t)I^{pr}(t+\tau)|^2 \, dt, \quad (4)$$

$$S^{(THz)}(\tau) = 2\alpha L \cos^2\Psi \frac{\omega^2}{\pi kc^2} \int e^{i\Omega\tau} \chi^{(2)}(\Omega)^2 \frac{(\Omega/c)^2}{k(\Omega)^2 - (\frac{\Omega}{v_g})^2} |C(\Omega)|^2$$

$$\times \left\{ e^{i[k(\Omega)-\Omega/v_g]z/2}\left[\text{sinc}\left(\left(k(\Omega) - \frac{\Omega}{v_g}\right)\frac{z}{2}\right) - 1 \right]\right\} d\Omega, \quad (5)$$

where L is the crystal length, $I^{pu,pr}(t) = |A^{pu,pr}(t)|^2$, and Ψ is the angle between the x axis and the linear polarization of the pump pulse. In Figs. 2a and 2c, we have plotted the temporal evolution of $S^{Kerr}(\tau)$ and $S^{THz}(\tau)$ for a $\langle 110 \rangle$ cut ZnTe and ZnSe crystal at $\Psi = 0°$, excited by a 100 fs laser pulse centered at 800 nm. The Fourier transform of the signal, $S^{THz}(\Omega)$ presented in Figs. 2b and 2d, allows one to evaluate the weight of each spectral component contributing to the index modulation at the end of the crystal. According to (5), the spectral density is the product of the THz wave spectrum with the optical probe (petahertz wave) integrated along the z axis and in time during the propagation. This figure clearly shows that, for ZnTe, the index modulation is peaked around the 2.3 THz phase-matched spectral component (i.e., $\Delta k^{THz} = 0$). This phase matching does not occur in the ZnSe spectrum (Fig. 2d) expressed in relative units versus the ZnTe signal.

Typical signals recorded in 2 mm $\langle 110 \rangle$ cut ZnTe crystals when the laser wavelength is tuned at 800 nm are presented in Fig. 3. These signals were recorded for a probe beam linearly polarized at 45° and for a pump beam linearly polarized along ($\Psi = 90°$, Fig. 3a) or perpendicular ($\Psi = 0°$, Fig. 3b) with respect to the $\langle 001 \rangle$ crystalline

axis. As we claim earlier, both n_2^{THz} and n_2^{Kerr} contributions are experimentally discriminated thanks to the symmetry of the second-order nonlinear coefficient. Indeed, when $\Psi = 90°$, the pump beam is polarized along the $\langle 001 \rangle$ axis; only n_2^{Kerr} accounts for the induced phase shift. The index change is then $\Delta\Phi(t) \sim n_2^{Kerr} I^{pu}(t)$. Therefore, according to (4), the measured heterodyne Kerr signal $S^{Kerr}(\tau) \sim \langle I^{pu}(t)I^{pr}(t+\tau)\rangle$ is proportional to the intensity autocorrelation function of the laser pulses. This gives access to the amplitude of n_2^{Kerr}. On the other hand, when the pump is polarized perpendicularly to this axis, the backaction of the THz radiation on the probe pulse occurs. Different behaviors have to be noted. First, the index change due to the THz wave is recorded even when the pump and probe beams are not temporally overlapped in the crystal; therefore the index change cannot be written by the classical expression $\Delta\Phi(t) = n_2^{THz} I^{pu}(t)$. This is in perfect agreement with our theoretical analysis which indicates that the induced index change is not temporally and spatially localized in the medium. Second, as expected we record a small signal before the pump pulse leaves the crystal. Third, the most important contribution at zero delay time is due to the optical Kerr effect signal. However,
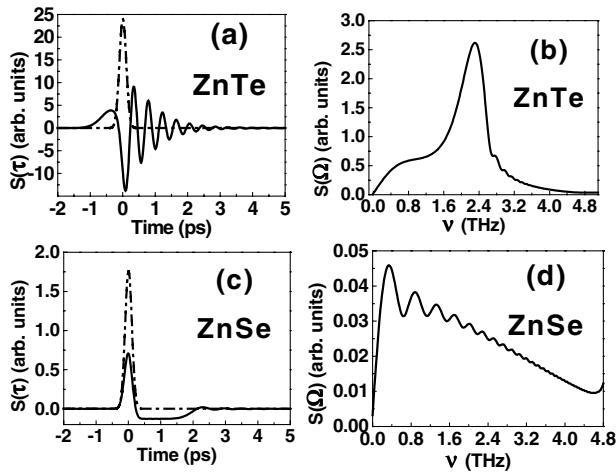
FIG. 2.　(a–c) Calculated temporal evolution of $S^{THz}(\tau)$ (solid lines) and $S^{Kerr}(\tau)$ (dash-dotted lines). (b–d): $S^{(Thz)}(\Omega)$ versus the phase mismatch $\Delta k^{THz}(\nu)$.

FIG. 3.　Signal $S(\tau)$ measured in ZnTe for (a) $\Psi = 90°$, (b) $\Psi = 0°$, (c) $\Psi = 40°$. (d) $S(\tau = 0)$ versus Ψ. (∘) experimental data, (—) theoretical fits, and (− · −) experimental noise level.

as expected this contribution rapidly decreases as the time delay between the pump and probe pulse increases, and oscillations at 2.39 THz clearly show up for the ZnTe Crystal. Again, these oscillations reveal the noninstantaneous character of $n_2^{THz}(\tau)$ in ZnTe crystal. When we changed the central laser frequency at 790 and 840 nm, the frequencies of recorded THz oscillations were 2.55 THz and 1.2 THz, respectively. This behavior is due to a shift of the phase-matched THz frequency and is in perfect agreement with the predicted values [7]. According to (4) and (5), we have fit the signal associated with $n_2^{Kerr}(\tau)$ and $n_2^{THz}(\tau)$ for ZnTe. A good fitting with the experimental data was found only by adjusting the amplitude of the heterodyne coefficient α, $u = \frac{\chi^{(3)}_{iiii}}{\chi^{(3)}_{iijj}}$, the ratio $r = \frac{\chi^{(3)}}{\chi^{(2)}\chi^{(2)}}$, and taking into account the important dispersion of the $\chi^{(2)}(\Omega)$ in these crystals in the THz spectral range. The solid lines in Fig. 3 present typical fits. The dispersion of $\chi^{(2)}(\Omega) = [\epsilon(\Omega)/\epsilon_0 - 1]$ was approximated from the Miller rules [11], where $\epsilon(\Omega)$ is the dielectric constant in the THz domain [12]. According to Fig. 2a and in agreement with our experimental data, at zero delay (i.e., $\tau = 0$) the contribution of n_2^{THz} is negligible. This makes it possible to evaluate u according to the measured signal $S(\tau = 0)$ when $0° < \Psi < 90°$ presented in Fig. 3c. In good agreement with theoretical work we found $u = 1.9$. The only remaining parameter to fix is the ratio $r = \frac{\chi^{(3)}}{\chi^{(2)}\chi^{(2)}}$. We found $r = 25$. The ratio $r = 37$ given by Table I neglects the dispersion of $\chi^{(2)} \sim \Omega^2$ and therefore gives a higher r value. However, when $0° < \Psi < 90°$, it is important to note that this latter analysis holds if, and only if, the coupling between third- and second-order nonlinear polarizations can be neglected. To evaluate the influence of this effect, we have numerically solved (3) by taking into account the parameters deduced from our simple analysis and computed the evolution of the signal. At $\Psi = 30°$, our simulations present a small difference of about 10% at
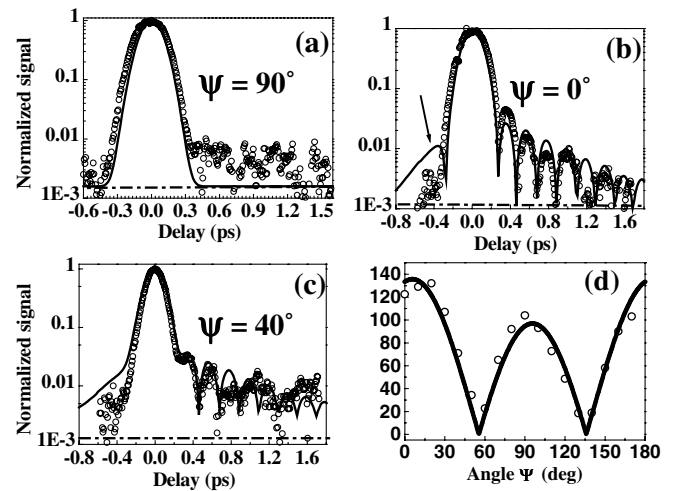
$\tau = 0$, indicating that our approximation is valid. The data recorded for the ZnSe crystal for $\Psi = 0°$ or $\Psi = 90°$ resemble Fig. 3a and further confirm our theoretical description. For this laser wavelength and for the temporal pulse width, no phase matching occurs for this crystal, and Δk is always positive for the THz spectrum. Therefore oscillations do not show up in the ZnSe crystal. Hence, n_2^{THz} is small compared to n_2^{Kerr} for this crystal. Moreover, according to Table I, the ratio $\frac{\chi^{(3)}}{\chi^{(2)}\chi^{(2)}}$ is greater than for ZnTe and therefore reduced the relative amplitude of n_2^{THz}.

In conclusion, we have experimentally evidenced the nonlinear refraction index n_2^{THz} resulting from the propagation of a THz wave in a zinc blende crystal. It has been shown experimentally and theoretically that n_2^{THz} is noninstantaneous and is maximum when $\Delta k^{THz} = 0$. This cascading effect should also be present in other nonlinear crystals such as KTP, KTA, LiNbO$_3$.

　*Electronic address: eric.freysz@cpmoh.u-bordeaux.fr

[1] L. A. Ostrowsky, JETP Lett. **5**, 272 (1967).
[2] R. DeSalvo *et al.,* Opt. Lett. **17**, 28 (1992).
[3] T. K. Gustafson *et al.,* Opt. Commun. **2**, 17 (1970).
[4] Ch. Bosshard *et al.,* Phys. Rev. Lett. **74**, 2816 (1995).
[5] I. Biaggio, Phys. Rev. Lett. **82**, 193 (1999).
[6] K. H. Yang, P. L. Richards, and Y. R. Shen, Appl. Phys. Lett. **19**, 285 (1971).
[7] A. Nahata, A. S. Weling, and T. F. Heinz, Appl. Phys. Lett. **69**, 2321 (1996).
[8] S. Montant *et al.,* J. Opt. Soc. Am. B **15**, 2802 (1998).
[9] S. A. Akhmanov, V. A. Vyslouck, and A. S. Chirkin, *Optics of Femtosecond Laser Pulses* (AIP, New York, 1992), Chap. 3, pp. 158–165.
[10] W. Y. Ching and M.-Z. Huang, Phys. Rev. B **47**, 9479 (1993).
[11] G. D. Boyd and M. A. Pollack, Phys. Rev. B **7**, 5345 (1973).
[12] T. Hattori *et al.,* Opt. Commun. **7**, 229 (1973).